Journal of Engineering Physics and Thermophysics, Vol. 75, No. 2, 2002

HYDROMAGNETIC CONVECTION FLOW THROUGH A POROUS MEDIUM IN A ROTATING CHANNEL

D. V. Krishna, D. R. V. Prasada Rao, and A. S. Ramachandra Murthy

UDC 536.25:537.84

An initial value investigation of the hydromagnetic convection flow of a viscous electrically conducting fluid through a porous medium in a rotating parallel plate channel has been made using boundary-layer-type equations. The exact solution of the governing equations is evaluated and the structure of the different boundary layers formed has been discussed in detail. The ultimate quasi-steady state velocity and temperature fields are numerically computed for various values of the governing parameters. Also the shear stress on the plates and the Nusselt numbers have been computed.

1. Introduction. The steady hydromagnetic rotating viscous flow through a non-porous or porous medium has drawn attention in recent years for possible applications in geophysical and cosmic fluid dynamics. For example, the channel flow problems where the flow is maintained by torsional or nontorsional oscillations of one or both boundaries throw some light in finding out the growth and development of boundary layers associated with flows occurring in geothermal phenomena. Claire Jacobs [1] has studied the transient effects considering the small amplitude torsional oscillations of disks. This problem has been extended to the hydromagnetic case by Murthy [3], who discussed torsional oscillations of the disks maintained at different temperatures. Debnath [2] has considered an unsteady hydrodynamic and hydromagnetic boundary flow in a rotating viscous fluid due to oscillations of plates including the effects of uniform pressure gradients and uniform suction. The structure of the velocity field and the associated Stokes, Ekman, and Rayleigh boundary layers on the plates are determined for the resonant and nonresonant cases. Rao et al. [5] have made an initial value investigation of the combined free and forced convection effects in an unsteady hydromagnetic viscous incompressible rotating fluid between two disks under a uniform transverse magnetic field. This analysis has been extended to porous boundaries by Sarojamma and Krishna [8] and later by Sivaprasad [11] to include the Hall current effects. Mishra and Narayana [9] have studied the unsteady free convective flow through a porous medium when the temperature of the plate is oscillating with time about a nonzero mean. Patil and Vadyanathan [4] have analyzed the fluid flow and the heat transfer in a rotating porous medium.

It is well known that in geothermal regions gases are electrically conducting and that they undergo the influence of a magnetic field. Keeping this in mind, Raptis [6] studied the unsteady MHD free convective flow of an electrically conducting fluid through a porous medium bounded by an infinite vertical and porous plate. In recent times, different problems related to transient convective flow through a porous medium have been discussed by Subba Bhatta [10] and Ravindra Reddy [7].

In this paper, we make an initial value investigation of the MHD mixed convection flow of a viscous fluid through a porous medium in a rotating parallel plate channel in the presence of a temperature-dependent heat source. The perturbations in the flow are created by a constant pressure gradient along the plates in addition to nontorsional oscillations of the lower plate. The exact solutions of the velocity and the temperature fields consist of the steady state and the transient components. The time required for the transient effects to decay is discussed in detail and the ultimate steady state consists of boundary layers on the plates and an interior. Attention is focused on the physical nature of the solutions and the structure of the various kinds of boundary layers formed on the plates. The final steady state velocity and temperature fields are numerically discussed for different values of the governing parameters. The shear stress and the Nusselt number are tabulated. The particular case where both plates are at rest has also been computed and analyzed.

Department of Mathematics, S. K. University, Anantapur – 515003, (A.P.) India. Published in Inzhenerno-Fizicheskii Zhurnal, Vol. 75, No. 2, pp. 12–21, March–April. Original article submitted July 17, 2001.

1062-0125/02/7502-0281$27.00

2. Formulation and Solution. We consider the unsteady flow of an incompressible, viscous fluid through a porous medium bounded by two parallel nonconducting plates under a uniform transverse magnetic field H_0. In the undisturbed state both the plates and the fluid rotate with the same angular velocity Ω. At $t > 0$, the fluid is driven by a constant pressure gradient parallel to the plate and in addition the lower plate performs nontorsional oscillations in its own plane. Further, the plates are cooled or heated by a constant temperature gradient in some direction parallel to the plane of the plates. We choose a Cartesian coordinate system $O(x', y', z')$ such that the plates are at $z' = 0$ and $z' = L$ and the Z-axis coincides with the axis of rotation of the plates. The unsteady hydrodynamic boundary-layer equations of motion with respect to a rotating frame moving with angular velocity Ω in the absence of any input electric field are

$$\frac{\partial u'}{\partial t'} - 2\Omega v' = -\frac{1}{\rho_0}\frac{\partial p'}{\partial x'} + \nu\frac{\partial^2 u'}{\partial z'^2} - \frac{\sigma\mu_e^2 H_0^2}{\rho_0}u' - \frac{\nu}{k}u', \tag{1}$$

$$\frac{\partial v'}{\partial t'} - 2\Omega u' = -\frac{1}{\rho_0}\frac{\partial p'}{\partial y'} + \nu\frac{\partial^2 v'}{\partial z'^2} - \frac{\sigma\mu_e^2 H_0^2}{\rho_0}v' - \frac{\nu}{k}v', \tag{2}$$

$$-\frac{1}{\rho_0}\frac{\partial p'}{\partial z'} - g\,(1 - \beta\,(T' - T_0)) = 0 \tag{3}$$

and the energy equation is

$$\left(\frac{\partial}{\partial t'} + u'\frac{\partial}{\partial x'} + v'\frac{\partial}{\partial y'}\right)(T' - T_0) = \alpha_1\frac{\partial}{\partial z'^2}(T' - T_0) + (Q/\rho_0 c_p)\,(T_0 - T)\,. \tag{4}$$

Combining Eqs. (1) and (2), we obtain

$$\frac{\partial q'}{\partial t'} - 2i\Omega q' - \nu\frac{\partial^2 q'}{\partial z'^2} + \frac{\sigma\mu_e^2 H_0^2}{\rho_0}q' + \frac{\nu}{k}q' = -\frac{1}{\rho_0}\left(\frac{\partial}{\partial x'} + i\frac{\partial}{\partial y'}\right)p' \tag{5}$$

where $q' = u' + iv'$.

Integrating (3), we get

$$p'/\rho_0 = -gz' + \beta g\int (T' - T_0)\,dz' + \phi\,(\xi', \bar{\xi}')\,H\,(t') \tag{6}$$

where $\xi' = x' - iy'$ and $\bar{\xi}' = x' + iy'$.

We use (3) in Eq. (5) and obtain

$$\frac{\partial}{\partial z'}\left[\frac{\partial q'}{\partial t'} - 2i\Omega q' - \nu\frac{\partial^2 q'}{\partial z'^2} + \left(\frac{\sigma\mu_e^2 H_0^2}{\rho_0} + \frac{\nu}{k}\right)q'\right] = -2\beta g\frac{\partial}{\partial \xi'}(T' - T_0)\,. \tag{7}$$

For the completeness of Eq. (7) we assume that

$$T' - T_0 = (Ax' + By')\,H\,(t') + \theta_1\,(z', t') \tag{8}$$

where A and B are the gradients of the temperature along $O(x', y')$ directions respectively, $\theta_1'(z', t')$ is an arbitrary function of z' and t', and $H(t')$ is the Heaviside function. Taking $T_0 + Ax' + By' + \theta'_{1\omega 1}$ and $T_0 + Ax' + + By' + \theta'_{1\omega 2}$ as the dimensional temperatures of the lower and upper plates, respectively, for $t > 0$, we obtain the following equation:

$$\left(\frac{\partial}{\partial t'} - 2i\Omega - \nu\frac{\partial^2}{\partial z'^2} + \frac{\sigma\mu_e^2 H_0^2}{\rho_0} + \frac{\nu}{k}\right) q' = \beta g\,(A + iB)\, z' H(t') + D \tag{9}$$

where

$$D = \frac{\partial}{\partial \xi'}\left[\phi(\xi', \bar{\xi}')\right] H(t') .$$

Introduction of the dimensionless variables

$$z = z'/L , \quad q = q'L/\nu , \quad t = t'\nu/L^2 , \quad \omega = \omega' L^2/\nu ,$$

$$\theta = \beta g L^3 (\theta_1' - \theta_{1\omega 1}')/\nu^2$$

yields the governing equations with respect to a rotating frame in the dimensionless form

$$\frac{\partial^2 q}{\partial z^2} - (\mathrm{Ha}^2 + \sigma_1^2 + 2i\mathrm{E}^{-1})\, q - \frac{\partial q}{\partial t} = \mathrm{Gr}\, z H(t) + R , \tag{10}$$

$$\frac{\partial^2 \theta}{\partial z^2} - \alpha\theta - \mathrm{Pr}\left[\frac{\partial \theta}{\partial t} + (\mathrm{Gr}_1 u + \mathrm{Gr}_2 v)\, H(t)\right] = 0 \tag{11}$$

where

$$\mathrm{E} = \nu/(\Omega L^2) , \quad \mathrm{Ha}^2 = \sigma L^2 \mu_e^2 H_0^2/(\rho\nu) , \quad \mathrm{Pr} = \mu c_p/k_1 , \quad \sigma_1^2 = L^2/k ,$$

$$\mathrm{Gr}_1 = \beta g A L^4/\nu^2 , \quad \mathrm{Gr}_2 = \beta g B L^4/\nu^2 , \quad \mathrm{Gr} = \mathrm{Gr}_1 + i\,\mathrm{Gr}_2 ,$$

$$R = (-L^3/\nu^2)\, D , \quad \alpha = QL^2/k_1 , \quad q = u + iv .$$

The boundary conditions in the dimensionless form are

$$q(z, t) = a \exp(i\omega t) + b \exp(-i\omega t) \quad \text{at} \quad z = 0 ,$$

$$q(z, t) = 0 \quad \text{at} \quad z = 1 ,$$

$$\theta(z, t) = 0 \quad \text{at} \quad z = 0 ,$$

$$\theta(z, t) = \beta g L^3 (\theta_{1\omega 2}' - \theta_{1\omega 1}')/\nu^2 = \theta_0 \quad \text{at} \quad z = 1 . \tag{12}$$

The initial conditions are $q(z, 0) = 0$ and $\theta(z, 0) = 0$.

Using Laplace transforms, the general solutions of (10) and (11) subjected to the boundary conditions (12) are

$$u + iv = \frac{(\mathrm{Gr} - R)\sinh\lambda_1 z}{\lambda_1^2 \sinh\lambda_1} + \frac{R\sinh\lambda_1 (z-1)}{\lambda_1^2 \sinh\lambda_1} - \frac{\mathrm{Gr}\, z - R}{\lambda_1^2} -$$

$$- \frac{a\sinh\lambda_2 (z-1)}{\sinh\lambda_2} \exp(i\omega t) - \frac{b\sinh\lambda_3 (z-1)}{\sinh\lambda_3} \exp(-i\omega t) -$$

$$- 2\,(\mathrm{Gr} - R)\sum_{n=1}^{\infty}\frac{(-1)^n \sin n\pi z}{n\pi\lambda_4^2}\exp(-\lambda_4^2 t) +$$

$$+\sum_{n=1}^{\infty}\left(\frac{a}{\lambda_4^2 + iw} + \frac{b}{\lambda_4^2 - iw} + \frac{R}{n\pi\lambda_4^2}\right)\sin n\pi\,(z-1)\exp(-\lambda_4^2 t)\,, \tag{13}$$

$$\theta = \theta_0 \sinh\sqrt{\alpha}\,z/\sinh\sqrt{\alpha} + 2\sum_{n=1}^{\infty}(-1)^n \sin n\pi z \exp(-(\alpha + n^2\pi^2 t/\mathrm{Pr})) +$$

$$+ \mathrm{Pr}\left\{\mathrm{Gr}_1 \operatorname{Re}\chi(z,t) + \mathrm{Gr}_2 \operatorname{Im}\chi(z,t)\right\} \tag{14}$$

where

$$\lambda_1^2 = \mathrm{Ha}^2 + \sigma_1^2 + 2i\mathrm{E}^{-1}\,;\quad \lambda_2^2 = \lambda_1^2 + i\omega\,;\quad \lambda_3^2 = \lambda_1^2 - i\omega\,;$$

$$\lambda_4^2 = n^2\pi^2 + \mathrm{Ha}^2 + \sigma_1^2 + 2i\mathrm{E}^{-1}\,.$$

The expression for χ has been evaluated but has not been mentioned due to its lengthiness.

3. Shear Stress and Rate of Heat Transfer. The dimensionless shear stresses τ_x and τ_y are obtained at the lower and upper plates from (13) and are given by

$$(\tau_x + i\tau_y)_{z=0} = \frac{\mathrm{Gr} - R + R\cosh\lambda_1}{\lambda_1 \sinh\lambda_1} - \frac{\mathrm{Gr}}{\lambda_1^2} - \frac{a\,\lambda_2 \cosh\lambda_2 \exp(i\omega t)}{\sinh\lambda_2} -$$

$$- \frac{b\,\lambda_3 \cosh\lambda_3 \exp(-i\omega t)}{\sinh\lambda_3}\,,$$

$$(\tau_x + i\tau_y)_{z=1} = \frac{\mathrm{Gr} - R + \cosh\lambda_1}{\lambda_1 \sinh\lambda_1} - \frac{\mathrm{Gr}}{\lambda_1^2} - \frac{a\,\lambda_2 \exp(i\omega t)}{\sinh\lambda_2} - \frac{b\,\lambda_3 \exp(-i\omega t)}{\sinh\lambda_3}\,.$$

The rate of heat-transfer coefficient (Nusselt number) on the plates is given by

$$(\mathrm{Nu})_{z=0} = \sqrt{\alpha}\cot\sqrt{\alpha} + \mathrm{Pr}\,\mathrm{Gr}\,Q_8\,,$$

$$(\mathrm{Nu})_{z=1} = \sqrt{\alpha}\,\operatorname{csch}\sqrt{\alpha} + \mathrm{Pr}\,\mathrm{Gr}\,Q_9$$

where

$$Q_1 = \frac{\mathrm{Gr}}{\lambda_1^2\lambda_5^2 \sinh\lambda_1} + \frac{\mathrm{Gr}}{\alpha\lambda_1^2} - \frac{\lambda_2 \cot\lambda_2 \exp(i\omega t)}{\lambda_1^2 + \omega_3^2}\,,$$

$$Q_2 = \frac{\sqrt{\alpha}\,(\alpha + \lambda_5^2)\cot\sqrt{\alpha}}{\alpha\lambda_1^2\lambda_5^2} + \frac{\omega_3 \cot\omega_2 \exp(i\omega t)}{\lambda_1^2 + \omega_3^2}\,,$$

$$Q_3 = \frac{\sqrt{\alpha}\,(\mathrm{Gr} - R)\,(\alpha + \lambda_5^2)}{\alpha\lambda_1^2\lambda_5^2 \sinh\sqrt{\alpha}},$$

$$Q_4 = \frac{(\mathrm{Gr} - R)\cot\lambda_1}{\lambda_1^2\lambda_5^2} + \frac{\mathrm{Gr}}{\alpha\lambda_1^2} - \frac{\lambda_2 \exp(i\omega t)}{\lambda_1^2 + \omega_3^2},$$

$$Q_5 = \frac{\sqrt{\alpha}\,(\alpha + \lambda_5^2)\cosh^2\sqrt{\alpha}}{\alpha\lambda_1^2\lambda_5^2 \sinh\sqrt{\alpha}} + \frac{\omega_2 \cosh^2\omega_2 \exp(i\omega t)}{(\lambda_5^2 + \omega_3^2)\sinh\omega_2},$$

$$Q_6 = \frac{\sqrt{\alpha}\,(\mathrm{Gr} - R)\,(\alpha + \lambda_5^2)}{\alpha\lambda_1^2\lambda_5^2}\cot\sqrt{\alpha},$$

$$Q_7 = \frac{R\sinh\sqrt{\alpha}}{\lambda_1^2\alpha^{3/2}} + \frac{\omega_2 \sinh\omega_2 \exp(i\omega t)}{(\lambda_5^2 + \omega_3^2)\sinh\omega_2},$$

$$Q_8 = \mathrm{Re}\,(Q_1 + Q_2 - Q_3), \quad Q_9 = \mathrm{Re}\,(Q_4 + Q_5 - Q_6 - Q_7),$$

$$\lambda_5^2 = \lambda_1^2\alpha, \quad \omega_1^2 = i\omega\,\mathrm{Pr}, \quad \omega_2^2 = \alpha + \omega_1^2; \quad \omega_3^2 = i\omega\,(1 - \mathrm{Pr}),$$

4. Discussion of the Associated Boundary Layers. We shall discuss the interplay between the Hartmann number Ha, the Ekman number E, and the porous parameter σ_1 in determining the time required for the decay of the transient terms in the solution. From (11), it follows that the transient velocity decays in dimensional time of order $1/(\pi^2 + \mathrm{Ha}^2 + \sigma_1^2)$. This implies that the decay time of transient velocity is less than the decay time in the absence of porosity of the medium.

The time required for the decay of the transient temperature is of order given by Max $\{(\mathrm{Ha}^2 + \sigma_1^2)^{-1}$, Pr/$\alpha$, $(1 - \mathrm{Pr})/(\mathrm{Ha}^2 + \sigma_1^2 - \alpha)\}$. In the steady-state limit the velocity distribution consists of two parts:

(i) The hyperbolic terms in z which give rise to layers of thickness of order $\{\mathrm{Ha}^2 + \sigma_1^2 + [(\mathrm{Ha}^2 + \sigma_1^2)^2 + (\omega - 2\mathrm{E}^{-1})^2]^{1/2}/2\}^{-1/2}$ near the plates through which the motion of the plate is communicated to the fluid.

(ii) The remaining terms represent an interior flow. We shall now discuss the role played by the Ekman number E, the Hartmann number Ha, and the porous parameter σ_1 in the determination of the layers formed on the plates. We shall consider the following cases of the frequency of oscillations:

(i) steady ($\omega = 0$);

(ii) low frequency ($\omega << 1$);

(iii) high frequency ($\omega >> 1$);

(iv) intermediate frequency ($\omega = \mathrm{O}(1)$).

(*i*) *Nonoscillatory Case* ($\omega = 0$) *or Low-Frequency Oscillations*

The solution represents the steady hydromagnetic boundary-layer flow superposed over a linear profile. The former consists of the Ekman–Darcy–Hartmann layer on both plates. This layer can be regarded as an Ekman–Darcy layer modified by the magnetic field or as an Ekman–Hartmann layer modified by porosity of the medium. When $\mathrm{E}^{-1} >> \sigma_1 >> \mathrm{Ha}$, the thickness of the boundary layer is $\mathrm{O}((\mathrm{E}^{-1} + \sigma_1^2)^{-1/2})$, which implies that in a porous medium the influence of the boundary gets confined to a thinner layer in comparison to the usual Ekman layer. When $\mathrm{E}^{-1} >> \sigma_1$ and $\mathrm{E}^{-1} >> \mathrm{Ha}$, the thickness of the layer is $\mathrm{O}((\mathrm{E}^{-1} + 2\sigma_1^2)^{-1/2})$, which shows that in the presence of a magnetic field of sufficiently large magnetic force in a porous medium with low permeability the thickness of the Ekman–Darcy layer is still more reduced, indicating that the influence of the boundary is confined to a comparably narrow region. When $\mathrm{E}^{-1} << \sigma_1$ and $\mathrm{E}^{-1} << \mathrm{Ha}$, the thickness of the boundary layer is $\mathrm{O}(1/\sigma_1)$ or $\mathrm{O}(1/\mathrm{Ha})$ according to whether $\sigma_1 > \mathrm{Ha}$ or $\sigma_1 < \mathrm{Ha}$. When $\mathrm{E}^{-1} << \mathrm{Ha}$ and $\sigma_1 << \mathrm{Ha}$ we find that the thickness of the layer is $\mathrm{O}(\mathrm{Ha}^2 + \mathrm{E}^{-1}/4\mathrm{Ha}^2)^{-1/2}$, which confirms that in the presence of the rotation the thickness of the Hartmann layer is reduced, and it is true even in the

TABLE 1. Phase of Resultant Velocity for Ha = 5, $\omega = 5$, $\sigma_1 = 2$, and E = 0.01

z \ Gr	10^3	$2\cdot10^3$	$3\cdot10^3$	$-3\cdot10^3$	$-2\cdot10^3$	-10^3
0.1	$64^o49'$	$84^o35'$	$178^o38'$	$319^o3'$	$330^o90'$	$335^o3'$
0.2	$78^o11'$	$167^o3'$	$178^o42'$	$344^o7'$	$344^o56'$	$345^o17'$
0.3	$165^o16'$	$165^o38'$	$165^o45'$	$346^o41'$	$346^o19'$	$346^o13'$
0.4	$165^o45'$	$165^o54'$	$169^o46'$	$346^o26'$	$346^o16'$	$346^o14'$
0.5	$166^o17'$	$166^o19'$	$166^o17'$	$346^o25'$	$346^o19'$	$346^o24'$
0.6	$166^o26'$	$166^o23'$	$166^o22'$	$346^o23'$	$346^o20'$	$346^o27'$
0.7	$164^o45'$	$164^o46'$	$164^o27'$	$344^o48'$	$344^o47'$	$344^o46'$
0.8	$158^o53'$	$158^o49'$	$174^o54'$	$338^o53'$	$338^o51'$	$338^o58'$
0.9	$146^o14'$	$146^o15'$	$146^o17'$	$326^o14'$	$326^o16'$	$326^o17'$

case of a porous medium of large permeability. When $E^{-1} >> Ha >> \sigma_1$, the boundary-layer thickness is $O((E^{-1} + Ha^2)^{-1/2})$, which is similar to the Ekman–Hartmann layer.

(*ii*) *High-Frequency Oscillations* ($\omega >> 1$)

It is observed from the solution that the boundary layer consists of a layer of thickness $O(1/\omega)$ when ω is much greater than E^{-1}, Ha, and σ_1. When $\omega \sim E^{-1}$ and $Ha >> E^{-1}$ and $\sigma_1 >> E^{-1}$, the thickness of the boundary layer is $O((Ha^2 + \sigma_1^2)^{-1/2})$, which corresponds to the Darcy–Hartmann layer. We get a boundary layer of thickness $O(E^{-1/2})$ for $\omega \sim E^{-1}$ and $E^{-1} >> Ha$ and $E^{-1} >> \sigma_1$. In this case, the viscous effect is felt in the entire fluid region if $2E^{-1} = \omega$. For $\omega \sim E^{-1}$ and $E^{-1} \sim Ha$, σ_1 the associated boundary layer is $O(\{Ha^2 + \sigma_1^2 + [Ha^2 + \sigma_1^2 + E^{-1}]^{1/2}\}^{-1/2})$ and for $\omega \sim E^{-1}$, $E^{-1} >> Ha$, and $E^{-1} >> \sigma_1$ the thickness is $O(E^{-1/2})$ which is similar to the Ekman layer.

(*iii*) *Intermediate-Frequency Oscillations* ($\omega = O(1)$)

In this case, the steady-state flow consists of a Darcy–Hartmann layer of thickness $O((E^{-1} + Ha^2)^{-1/2})$ when Ha and σ_1 are much greater than E^{-1} and ω, and it is $O((\omega^{-2}E^{-1})^{-1/2})$ when Ha and σ_1 are much less than E^{-1}. This shows that the viscous effects pervade all over the fluid region if $\omega \sim 2E^{-1}$. If $\omega = 2E^{-1}$ and Ha, $\sigma_1 \sim O(1)$, then the thickness is of order $O((Ha^2 + \sigma_1^2)^{-1/2})$. When $\omega \sim O(1)$ and $\omega E \geq 1$ the thickness reduces to $O([\omega^2E^{-2} + (Ha^2 + \sigma_1^2)^{1/2} + Ha^2 + \sigma_1^2]^{-1/2})$ and this of order $O(\omega E^{-1})$ provided $\omega >> Ha$ and $\omega >> \sigma_1$.

5. Discussion of the Computational Analysis. The quasisteady parts of the velocity and temperature representing the ultimate flow have been computed numerically for different sets of governing parameters Gr, Ha, σ_1, α, and ω, and their profiles are plotted in Figs. 1–12. For computational purposes we have assumed Gr to be real so that the applied pressure gradient in the *y*-direction is zero and Gr is positive or negative depending on whether the plates are heated or cooled along the direction of the *x*-axis (nonzero pressure gradient). Also the Prandtl number Pr is chosen to be Pr = 0.71. Since the thermal buoyancy balances the vertical pressure gradient in the absence of any other applied force in the direction of rotation, the flow takes place in planes parallel to the boundary plates. However the flow is three-dimensional and all the perturbed variables have been obtained using boundary-layer-type equations, which would reduce to two coupled partial differential equations for a complex velocity and the real temperature.

Figures 1–7 correspond to profiles when one of the plates (lower) is oscillating with a given amplitude and other is at rest. Figures 8–12 correspond to the profiles when both plates are at rest. We observe from Figs. 1 and 2 that in general *u* and *v* carry opposite signs for all Gr positive or negative. However, for $Gr > 0$ the resultant flow (Table 1) is directed towards the axis of zero pressure gradient (*y*-axis) with the positive obtuse phase angle relative to the *x*-axis. When $Gr < 0$, the same resultant flow is directed towards the nonzero pressure gradient axis (*x*-axis) with the negative obtuse phase angle. The magnitudes of *u* and *v* increase with |Gr| (Figs. 1 and 2) and hence the resultant velocity increases in its magnitude with |Gr|. Figures 3 and 4 indicate the behavior of the velocity components *u* and *v* with variations in Ha, σ_1, ω, and E. We note that individually *u* exhibits a slight enhancement in contrast to *v*, which retards appreciably with increase in Ha and ω. Value of *u* experiences a fluctuation, while *v* shows a definite retardation with increase in σ_1. An increase in E marks a significant growth, although *v* experiences retardation. De-

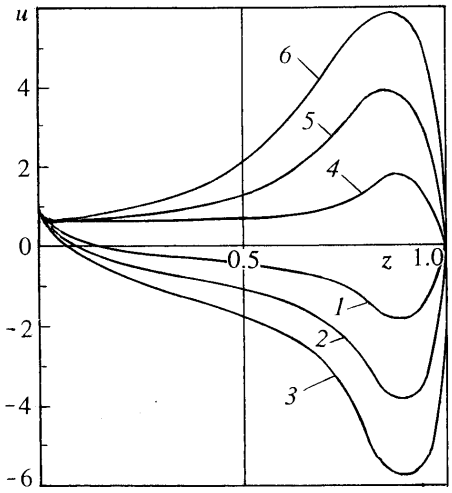

Fig. 1. Profiles of dimensionless axial velocity u for the oscillating lower plate at different Gr: 1) Gr = 10^3; 2) $2 \cdot 10^3$; 3) $3 \cdot 10^3$; 4) -10^3; 5) $-2 \cdot 10^3$; 6) $-3 \cdot 10^3$.

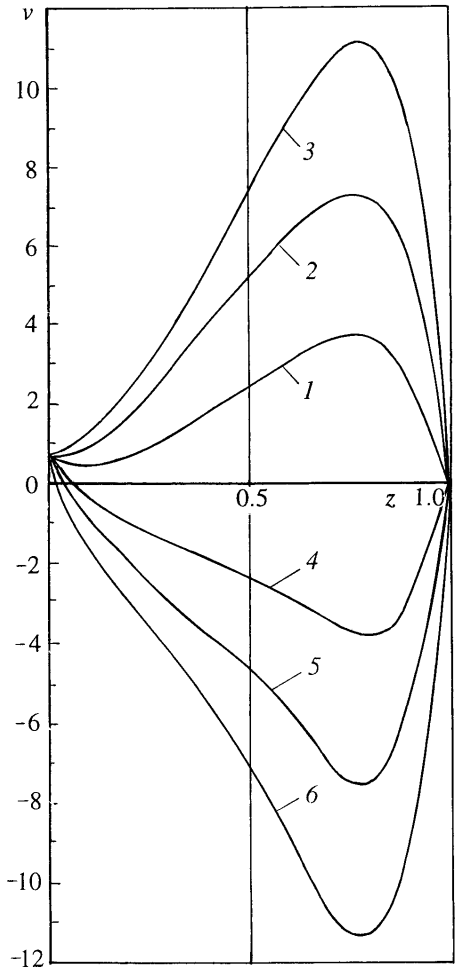

Fig. 2. Profiles of dimensionless transverse velocity v for the oscillating lower plate at different Gr. For notation see Fig. 1.

spite these individual variations, it is interesting to note that the resultant velocity (Fig. 5) experiences a retardation with increase in Ha, σ_1, and ω, while it exhibits an appreciable enhancement with increase in E. The retardation due to an increase in the porous parameter is more rapid than that due to the increase in the Hartmann number. In other

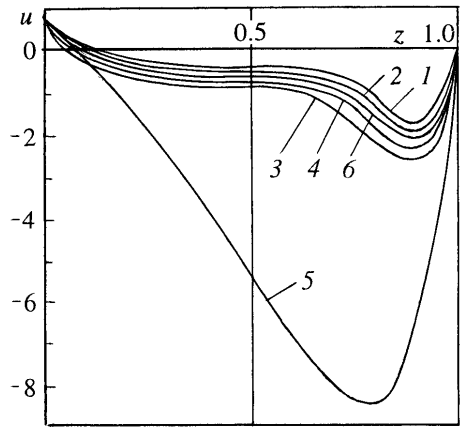

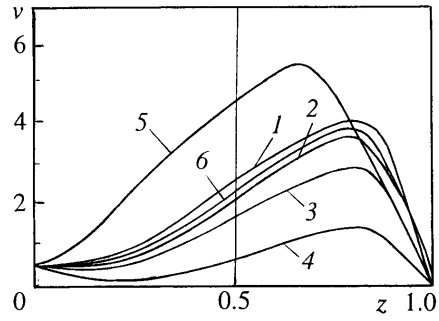

Fig. 3. Profiles of dimensionless axial velocity u for the oscillating lower plate: 1) Ha = 5, σ_1 = 5, ω = 2, and E = 0.01; 2) 10, 5, 2, and 0.01; 3) 5, 2, 2, and 0.01; 4) 5, 10, 2, and 0.01; 5) 5, 5, 2, and 0.05; 6) 5, 5, 5, and 0.01.

Fig. 4. Profiles of dimensionless transverse velocity v for the oscillating lower plate. For notation see Fig. 3.

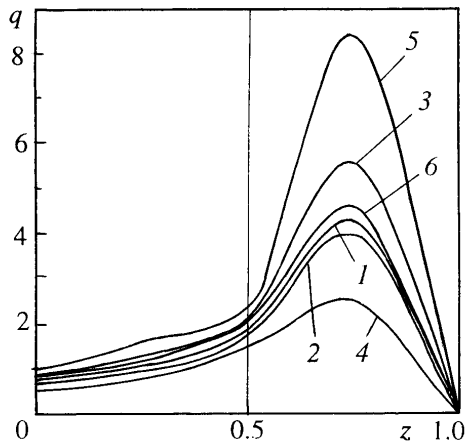

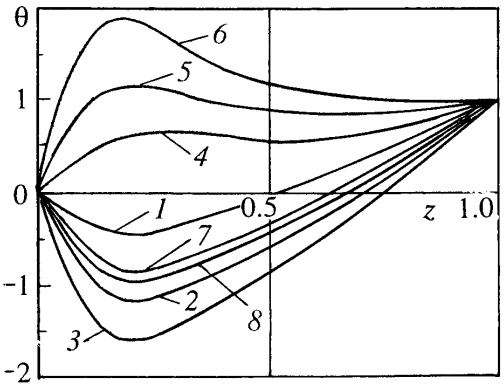

Fig. 5. Profiles of dimensionless resultant velocity q for the oscillating lower plate. For notation see Fig. 3.

Fig. 6. Profiles of dimensionless temperature θ for the oscillating lower plate: 1) Gr = 10^3 and σ_1 = 5; 2) $2\cdot10^3$ and 5; 3) $3\cdot10^3$ and 5; 4) -10^3 and 5; 5) $-2\cdot10^3$ and 5; 6) $-3\cdot10^3$ and 5; 7) $2\cdot10^3$ and 10; 8) $2\cdot10^3$ and 15.

words, the resistance offered by the porosity of the medium is much more than the resistance due to the magnetic lines of force.

Similar observations are made when both boundaries are at rest. We find that the resultant velocity increases with |Gr| (Fig. 10) and E, whereas it decreases with an increase in Ha and σ_1.

The behavior of the temperature may be analyzed from Figs. 6 and 7. When Gr > 0 we find (Fig. 6) that actual temperature decreases from its prescribed value on the lower boundary to some minimum attained at an axial distance of 0.2 and later increases to reach its prescribed value on the upper plate. In the former case (Gr > 0), it is interesting to note that when Gr increases, the low-temperature region spreads gradually from the lower half to the upper half when the temperature decreases rapidly with increase in Gr in the entire flow region. In contrast, with an

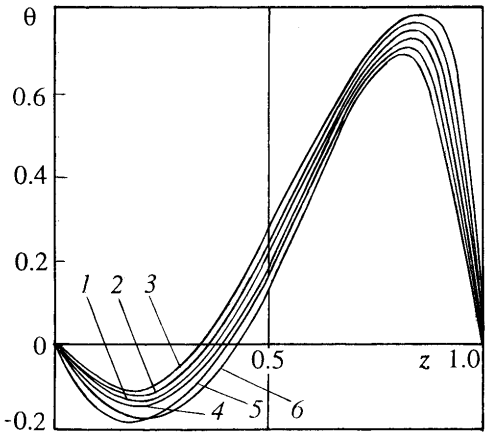

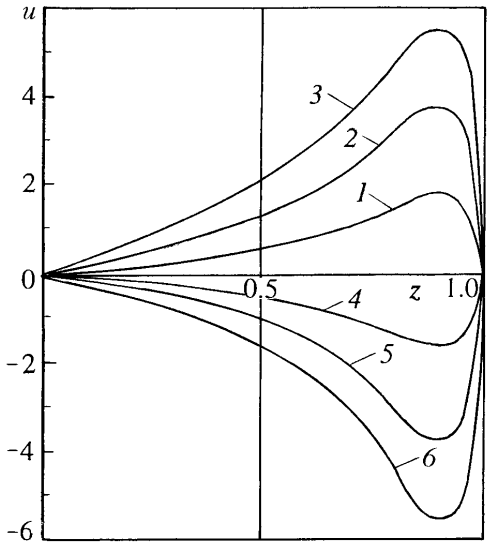

Fig. 7. Profiles of dimensionless temperature θ for the oscillating lower plate: 1) Ha = 5, ω = 2, α = 5, and E = 0.01; 2) 10, 2, 5, and 0.01; 3) 5, 10, 5, and 0.01; 4) 5, 2, 10, and 0.01; 5) 5, 2, 15, and 0.01; 6) 5, 2, 5, and 0.05.

Fig. 8. Profiles of dimensionless axial velocity u for plates at rest at different Gr. For notation see Fig. 1.

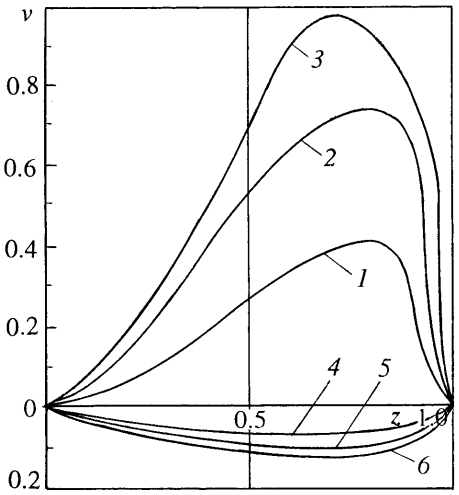

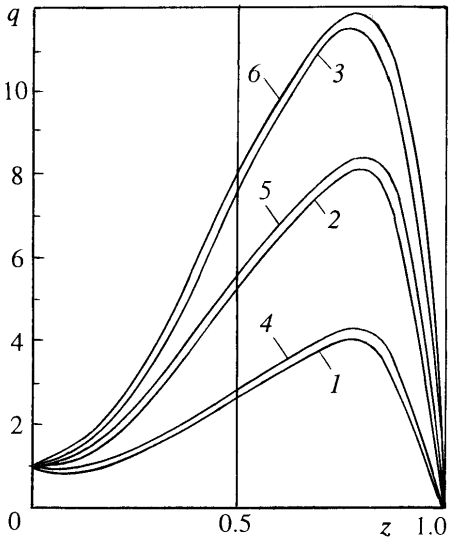

Fig. 9. Profiles of dimensionless transverse velocity v for plates at rest at different Gr. For notation see Fig. 1.

Fig. 10. Profiles of dimensionless resultant velocity q for plates at rest at different Gr. For notation see Fig. 1.

increase in |Gr| (for Gr < 0), the actual temperature increases at all corresponding points in the flow region. Also, it increases for an increase in the porous paramter σ_1 in the flow region. Figure 7 indicates the behavior of the perturbed temperature θ for variations in Ha, ω, α, and E. From the profiles we see that the actual temperature increases with Ha and ω. Likewise, for an increase in the heat-source parameter α, the temperature decreases near the lower plate while it increases in the rest of the region. The temperature also decreases with increase in E in the whole region.

The shear stress and the rate of heat transfer (Nusselt number) is given in Tables 2–4. The magnitude of these stresses at the stationary upper plate is significantly high compared to the respective magnitudes at the oscillating lower plate. Both τ_x and τ_y slightly reduce at the upper plate whereas they enhance at the lower plate with Ha and σ_1 (Table 2). The retardation at the upper plate is significantly low compared to the enhancement at the lower plate. Also, τ_x rapidly increases while τ_y reduces with E at either boundaries. An increase in |Gr| (Gr > 0 or Gr < 0) en-

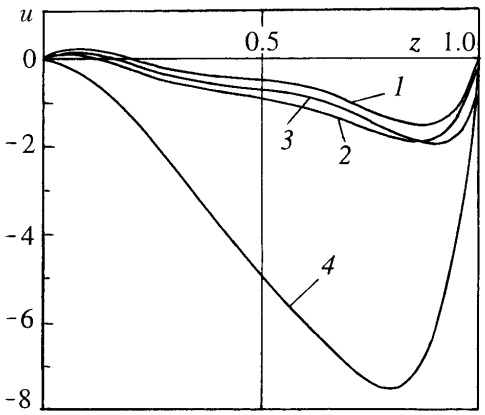

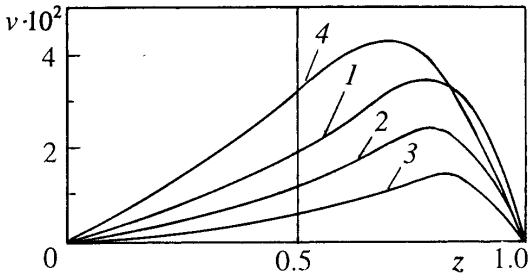

Fig. 11. Profiles of dimensionless axial velocity u for plates at rest: 1) Ha = 5, σ_1 = 5, and E = 0.01; 2) 10, 5, and 0.01; 3) 5, 10, and 0.01; 4) 5, 5, and 0.05.

Fig. 12. Profiles of dimensionless transverse velocity v for plates at rest. For notation see Fig. 11.

TABLE 2. Shear Stresses at the Plates

Gr	$5\cdot10^2$	10^3	$-5\cdot10^2$	-10^3	$5\cdot10^2$	$5\cdot10^2$	$5\cdot10^2$	$5\cdot10^2$
σ_1	5	5	5	5	10	5	5	5
Ha \ E	0.01	0.01	0.01	0.01	0.01	0.001	0.01	0.3
τ_x at the upper plate								
2	28.80483	53.66465	–26.91489	–48.40278	27.29567	26.80490	58.1418	60.2681
5	27.29567	54.64835	–27.40967	–49.29181	26.16216	27.29568	40.3108	40.5955
10	25.09653	50.24580	–25.20201	–45.32142	23.46271	25.09653	29.4968	29.5525
τ_y at the upper plate								
2	–19.03471	–38.11259	19.12105	34.38336	–13.95359	–19.03474	–9.40543	–3.34614
5	–13.95359	–27.93874	14.01672	25.20484	–10.10450	–2.8905	–2.89050	–0.97547
10	–8.25556	–16.52962	8.29255	14.91180	–6.27008	–8.2556	–1.09838	–0.36731
τ_x at the lower plate								
2	–2.33521	–2.9242	–1.15705	–0.68579	–5.34016	–2.30257	–12.66096	–14.31193
5	–5.34026	–6.4637	–3.09295	–2.19406	–7.66425	–5.27073	–11.14355	–11.62517
10	–8.94756	–10.1670	–6.50854	–5.53293	–10.6215	–8.85272	–12.68857	–12.98849
τ_y at the lower plate								
2	–11.96866	–9.61565	–16.67467	–18.55707	–13.02930	–12.24150	–2.84333	–4.20110
5	–13.02936	–11.23170	–16.62467	–18.06280	–14.34495	–13.27756	–8.00732	–7.97324
10	–15.20412	–14.22851	–17.15534	–16.50998	–16.41356	–15.40515	–11.52538	–11.32421

TABLE 3. Dependence of Nusselt Number at the Plates on Ha, Gr, σ_1, and α

Gr	$5\cdot10^2$	10^3	$-5\cdot10^2$	-10^3	$5\cdot10^2$	$5\cdot10^2$	$5\cdot10^2$	$5\cdot10^2$	$5\cdot10^2$
σ_1	5	5	5	5	10	15	5	5	5
Ha \ α	5	5	5	5	5	5	10	15	20
upper plate									
2	2.7183	3.3777	4.5127	1.8645	1.2432	–0.2437	3.0275	5.2341	7.9296
5	2.6213	3.0274	3.4531	1.9039	1.2340	–0.1338	2.8791	3.6476	5.8641
10	2.5692	2.8538	2.9617	1.9331	1.2634	–0.2191	2.8622	2.7832	2.8916
lower plate									
2	20.2667	49.8712	99.3583	–19.2438	–48.8050	–97.9940	47.1056	52.6512	57.7514
5	19.1276	47.1056	93.7671	–18.1543	–46.0992	–92.6426	45.8195	50.9174	55.6089
10	18.4680	45.4445	90.4041	–17.5013	–44.4788	–89.4429	45.2773	49.4465	54.5727

hances the stresses on the stationary plate, but on the oscillating plate τ_x experiences a slight enhancement with |Gr| for $Gr > 0$ and retardation for $Gr < 0$. The reverse behavior is observed for τ_y.

The Nusselt number (Nu) at the upper and lower plates is given in Tables 3 and 4 for variations in Gr, σ_1, α, Ha, E, and ω. We observe that the magnitudes of Nu at the oscillating lower plate for different values of the said parameters are fairly high in comparison to the respective values at the stationary upper plate. An increase in Gr for $Gr > 0$ enhances Nu at both boundaries, although the enhancement at the oscillating plate is quite significant compared to its growth at the stationary plate. In contrast, an increase in |Gr| for $Gr < 0$ reduces Nu at either boundary and the

TABLE 4. Dependence of Nusselt Number at the Plates on Ha, ω, and E

ω	2	5	10	20	2	2	2	2
Ha \ E	0.01	0.01	0.01	0.01	0.001	0.1	0.3	0.5
upper plate								
2	2.7183	2.5353	2.4187	2.4389	3.3335	−1.9565	−3.9844	−4.3104
5	2.6213	2.2085	2.0934	2.1134	3.3251	1.36005	1.2809	1.2734
10	2.5692	2.0565	1.9445	1.9446	3.3113	2.4113	12.4002	2.3987
lower plate								
2	20.2267	17.8678	7.7956	3.2613	160.5124	11.9567	7.9476	7.2155
5	19.1277	17.9461	7.9637	3.3440	157.7720	18.1405	15.9561	15.5290
10	18.4680	19.0814	8.7652	3.7552	153.3780	24.1287	22.6140	22.3119

reduction is notable at the oscillating plate, as in the preceding case. Also the rate of heat transfer reduces with increase in Hartmann number at either boundary for all variations in other parameters. However, other parameters being fixed, an increase in the heat source parameter enhances Nu at either boundary. The lower the permeability of the medium (corresponding to increase in σ_1), the higher the rate of heat transfer at the oscillating plate and the less at the stationary plate. We also observe that Nu reduces in general with increase in E or ω on either plate (Table 3), except for the stationary plate for higher $\omega \approx 20$.

NOTATION

z', axis of rotation; x' and y', dimensional coordinates along and normal to the plane; x and y, dimensionless coordinates along and normal to the plane; t, dimensionless time; L, characteristic length; a, b, coefficients of the imposed nontorsional oscillations; u and v, dimensionless axial and transverse velocity components; T_0, characteristic temperature; $H(t)$, Heaviside step function; E, Ekman number; Ha, Hartmann number; Pr, Prandtl number; Gr_1 and Gr_2, Grashof numbers along x and y directions; R, pressure gradient parameter; Nu, Nusselt number; Q, strength of the heat source; k, permeability of the porous medium; p', pressure; k_1, thermal conductivity; ρ_0, density of the fluid in the equilibrium state; β, coefficient of volume expansion; c_p, specific heat at constant pressure; σ, electrical conductivity; σ_1, porous parameter; μ, coefficient of viscosity; μ_e, magnetic permeability; Ω, angular velocity; ω, frequency of the nontorsional oscillations; τ_x and τ_y, dimensionless shear stresses along x and y directions; α, dimensionless heat source parameter; α_1, thermal diffusivity; ν, coefficient of kinematics viscosity; θ, dimensionless temperature; $\theta'_{1\omega 1}$ and $\theta'_{1\omega 2}$, prescribed values of θ_1 on the lower and upper plates.

REFERENCES

1. C. Jacobs, *QJMM*, **24**, 221–230 (1971).
2. L. Debnath, *ZAMM*, **65**, 431–435 (1975).
3. K. N. V. Murthy, *Appl. Sci. Res.*, **35**, 111–115 (1979).
4. P. Patil and G. Vidyanathan, *Int. J. Eng. Sci.*, **21**, No. 2, 124–130 (1983).
5. D. R. V. Rao, D. V. Krishna, and L. Debnath, *Acta Mech.*, **34**, 225–240 (1982).
6. A. A. Raptis, *Energy Res.*, **10**, 97–101 (1986).
7. A. R. Reddy, *Computational Techniques in Hydromagnetic Convective Flows through Porous Medium*, Ph.D. Dissertation, Anantapur, India (1997).
8. G. Sarojamma and D. V. Krishna, *Acta Mech.*, **40**, 277–288 (1981).
9. P. Singh, J. K. Mishra, and K. A. Narayana, *Int. J. Eng. Sci.*, **24**, No. 2, 227–232 (1986).
10. S. M. C. V. Subba Bhatta, *MHD Transient Convection Flow through a Porous Medium*, Ph.D. Dissertation, Anantapur, India (1996).
11. R. Sivaprasad, *Convection Flows in Magnetohydrodynamics*, Ph.D. Dissertation, Anantapur, India (1985).